JCI insight

# Exhausted-like CD8 T cell phenotypes linked to C-peptide preservation in alefacept-treated T1D subjects

Kirsten E. Diggins, … , S. Alice Long, Peter S. Linsley

*JCI Insight.* 2020. https://doi.org/10.1172/jci.insight.142680.

**Research** In-Press Preview **Immunology**

Clinical trials of biologic therapies in type 1 diabetes (T1D) aim to mitigate autoimmune destruction of pancreatic beta cells through immune perturbation and serve as resources to elucidate immunological mechanisms in health and disease. In the T1DAL trial of alefacept (LFA3-Ig) in recent onset T1D, endogenous insulin production was preserved in 30% of subjects for two years post-therapy. Given our previous findings linking exhausted CD8 T cells to beneficial response in T1D trials, we applied unbiased analyses to sorted CD8 T cells to evaluate their potential role in T1DAL. Using RNA-seq, we found that greater insulin C-peptide preservation was associated with a module of activation- and exhaustion-associated genes. This signature was dissected into two distinct CD8 memory populations through correlation with clustered cytometry data. Both populations were hypo-proliferative, shared expanded TCR junctions, and expressed exhaustion-associated markers including TIGIT and KLRG1. The populations were distinguished by reciprocal expression of CD8 T and NK cell markers (GZMB, CD57 and inhibitory KIR genes), versus T cell activation and differentiation markers (PD1 and CD28). These findings support previous evidence linking exhausted CD8 T cells to successful immune interventions for T1D, while suggesting multiple inhibitory mechanisms can promote this beneficial cell state.



# Exhausted-like CD8 T cell phenotypes linked to C-peptide preservation in alefacept-treated T1D subjects

**Authors:** Kirsten E. Diggins[1†], Elisavet Serti[2†], Virginia Muir[1], Mario Rosasco[1], TingTing Lu[2], Elisa Balmas[3], Gerald Nepom[2], S. Alice Long[3], and Peter S. Linsley[1*]

**Affiliations:**

[1]Systems Immunology, Benaroya Research Institute at Virginia Mason

[2]Immune Tolerance Network (ITN), Bethesda, MD

[3]Translational Immunology, Benaroya Research Institute at Virginia Mason, Seattle, WA

*Corresponding authors: Peter S. Linsley; plinsley@benaroyaresearch.org; 1201 9th Ave, Seattle, WA 98101; Phone: (206) 342-6947

†These authors contributed equally to this work.

All authors declare no conflict of interest.

## Abstract

Clinical trials of biologic therapies in type 1 diabetes (T1D) aim to mitigate autoimmune destruction of pancreatic beta cells through immune perturbation and serve as resources to elucidate immunological mechanisms in health and disease. In the T1DAL trial of alefacept (LFA3-Ig) in recent onset T1D, endogenous insulin production was preserved in 30% of subjects for two years post-therapy. Given our previous findings linking exhausted-like CD8 T cells to beneficial response in T1D trials, we applied unbiased analyses to sorted CD8 T cells to evaluate their potential role in T1DAL. Using RNA-seq, we found that greater insulin C-peptide preservation was associated with a module of activation- and exhaustion-associated genes. This signature was dissected into two CD8 memory phenotypes through correlation with cytometry data. These cells were hypo-proliferative, shared expanded rearranged TCR junctions, and expressed exhaustion-associated markers including TIGIT and KLRG1. The two phenotypes could be distinguished by reciprocal expression of CD8 T and NK cell markers (GZMB, CD57 and inhibitory KIR genes), versus T cell activation and differentiation markers (PD1 and CD28). These findings support previous evidence linking exhausted-like CD8 T cells to successful immune interventions for T1D, while suggesting multiple inhibitory mechanisms can promote this beneficial cell state.

## Introduction

Type 1 diabetes (T1D) is an autoimmune disease in which β cells of the pancreas are destroyed, resulting in a lifelong dependence on exogenous insulin (1). As some residual beta cell function is present upon diagnosis, preserving remaining beta cell function is the primary therapeutic goal when treating recent onset (RO) T1D. The goal of immunotherapies is to establish and maintain a tolerogenic immune state. While no therapies to date have preserved beta cell function beyond one year in all treated RO T1D subjects (2-19), a subset of subjects respond better than others in many of these trials. Understanding immune states and immunological changes associated with treatment and outcome can help improve tolerance-inducing strategies that prolong clinical benefit.

An emerging mechanism in slower autoimmune disease progression (20) and better response to therapy is T cell exhaustion (21, 22). An expansion of TIGIT+KLRG1+ (Double Positive, or DP) CD8 T cells, described as "partially exhausted", was linked to good clinical outcome in trials of anti-CD3 mAb teplizumab in RO and at-risk subjects in T1D (22). Other successful biologic therapies for T1D did not trigger obvious accumulation of DP cells (23, 24), nor were they observed in bulk transcript profiles from untreated subjects (25), demonstrating context-specificity. However, exhausted autoreactive CD8 T cells were also linked to rate of progression in established T1D diabetes (26).

Alefacept is a LFA-3-Ig fusion protein that binds CD2 (27), disrupts CD58-mediated co-stimulation of T cells (28), and selectively depletes memory/effector T cells (29-33) via NK-mediated antibody mediated cytotoxicity (ADCC) (31). The T1DAL study was a phase 2, double-blind, placebo-controlled trial of alefacept in RO T1D patients diagnosed within 100 days leading up to enrollment in the trial. Alefacept resulted in significant preservation of endogenous insulin production in 30% of treated subjects after two years compared with placebo (11, 15). Alefacept treatment altered immunological profiles and induced potentially tolerogenic changes in the T cell compartment. CD4 effector memory (TEM) and central

memory (TCM) T cells were depleted and CD4 FOXP3+CD127lo regulatory T cells (TREG) were preserved, resulting in an increased ratio of TREG to memory T cells.

Given that exhausted CD8 T (TEX) cells have been associated with response to other T-cell targeting therapies (22), we explored the possibility that alefacept had immunomodulatory effects on residual CD8 T cells by performing detailed analysis of the phenotype and function of CD8 T cells following therapy and relating their biological signatures with clinical outcome. Using integrated RNA-sequencing and CyTOF analysis. We identify and describe two CD8 phenotypes that correlated with clinical response; one defined by higher CD57 expression that was maintained and another defined by high levels of PD-1 expression that recovered post-treatment in treatment responders. These cells were phenotypically distinct from one another, but both shared characteristics of the DP cells previously seen in responders to teplizumab (anti-CD3) in the AbATE trial, including high inhibitory receptor (IR) expression and hypoproliferation following to anti-CD3/anti-CD28 stimulation. These results expand on the evidence that therapeutic modulation of CD8 populations with features of exhaustion or terminal differentiation are linked to preservation of beta cell function in T1D.

## Results

Alefacept was shown to deplete CD2hi CD4 and CD8 T effector and memory subsets in all subjects in the T1DAL trial; however, these changes were not associated with therapy response as measured by maintenance of beta cell function (15). While most T cell populations were depleted consistently across all subjects, the CD8 effector memory (TEM) cells showed notable variability in extent of depletion, suggesting that differential changes related to response could exist in this compartment. Additionally, previous evidence indicated that expansion of exhausted CD8 T cells was linked to better outcome in T1D clinical trials of biologic agents (22). We therefore hypothesized that phenotypic and functional changes occurring post-treatment in T1DAL subjects' CD8 T cells would identify biologically and therapeutically relevant signatures of response.

To address this hypothesis, we obtained frozen PBMC that were isolated from trial subjects at five time points: immediately before treatment, twice during the course of treatment, and twice up to 2 years post-treatment (Figure 1A). As previously described (11, 15), 49 RO T1D subjects were enrolled and randomly assigned to receive alefacept (n=33) or placebo (n=16). Sorted CD8 T cells from 30 of these subjects were analyzed by bulk RNA-seq (Materials and Methods). Following quality control and filtering, transcript data from 26 of these subjects was included in gene expression analysis. Additionally, PBMCs from treated and placebo subjects were analyzed by flow and mass cytometry (Table 1). Subjects were selected to maximize response variability and therefore included subjects with greatest C-peptide preservation (responders) or loss (non-responders) at week 104 (Materials and Methods). Neither the RNA-seq nor the cytometry cohorts differed significantly from the original cohort of 33 subjects in terms of age, sex, and response (Table 1) (15).

*A CD8 T cell activation and exhaustion-related gene signature was associated with response to alefacept:*

We applied Weighted Correlation Network Analysis (WGCNA) to post-processed gene counts in order to discover modules of co-regulated genes via an unsupervised approach (34). WGCNA is an unbiased clustering method that identifies sets, or modules, of correlated genes with the assumption that genes whose expression is highly correlated are likely involved in the same biological functions or pathways. We reasoned that WGCNA would identify immunological pathways or functions that were linked to therapy response. The analysis included samples from the end of the trial (2 years post-treatment) given that the greatest disparity existed in outcomes at this time point. This also enabled evaluation of long-term remodeling of the CD8 T cell compartment that might point to persisting, long-term alterations related to better response.

We performed WGCNA on the top 5000 most variable genes across all available week 104 samples (n = 24; see Materials and Methods and Table S1). The analysis identified six distinct gene modules, ranging in size from 62 to 738 genes (Figure 1B). An additional module, labeled as the gray module by WGCNA, included the remaining, uncorrelated genes. Module eigengenes (weighted combination of module genes' expression levels) were correlated with C-peptide change (defined as the slope from random-effects model fitted to 4 hour AUC from baseline through the end of trial; see Materials and Methods). Of these seven modules, only the blue module was significantly correlated with response (n = 738 genes; correlation p-value $< 0.05$), indicating that higher expression of the genes in this module occurred in subjects with prolonged C-peptide preservation (Figure 1C-D). Given that higher blue module gene expression was seen in those with better outcomes at the end of the trial, we wanted to evaluate if this difference occurred only 2 years post treatment or showed divergence between groups earlier in the trial. To evaluate the dynamics of blue module expression over the course of the trial, change from baseline median module gene expression was determined for all available samples per visit (Table S1; Figure 1E). Median blue module gene expression declined in non-responders at week 52, while remaining higher in responders over the

course of the trial (Figure 1E). This module was not correlated with age (Figure S1), indicating that increased expression of these genes was not the result of an age-related immune state.

Gene Ontology (GO) analysis was applied to the blue module to identify enriched functional pathways within the gene set. Of the 837 significantly enriched GO terms (FDR < 0.01), 114 terms were related to T cell activation, differentiation, cytotoxicity, and apoptosis (Figure 1G). These terms included the genes *CD38*, *EOMES*, *GZMB*, *TIGIT*, *LAG3*, *KLRD1*, *CD160*, among other IR genes and genes associated with T cell activation responses (Figure 1G). Because of the high diversity of functional pathways associated with blue module genes, we hypothesized that the response signature could be arising from more than one CD8 T cell population.

*Increased frequency of CD8 TEM populations with high IR expression was associated with beneficial clinical response to alefacept:*

First, we evaluated the CD8 TEM populations expressing cytotoxic and exhaustion-associated markers by flow cytometry analysis (Figure S2), given that the gene signature identified by WGCNA included many IR genes, as well as previous evidence that exhausted-like cells have been associated with immunotherapeutic response in T1D (22). Within the CD8 TEM compartment (CD45RO+ CCR7-; Figure S2), there was an increased frequency of cells that were KLRG1+TIGIT+, CD57+, or Granzyme B+, with the highest frequencies found in subjects with favorable clinical outcomes (Figure 2A). The change in frequency of these cells from baseline to the end of the trial correlated with the rate of change of C-peptide in treated subjects (Figure 2B) but not in placebo subjects (Figure S3), suggesting that maintenance or relative increases in these CD8 TEM phenotypes may contribute to the role of alefacept in preserving beta cell function. This association with response was specific to CD8 T cells, as neither the change in total NK cell frequency (CD3- CD56+) nor CD57+ NK cell frequency (CD3- CD56dim CD57+) differed between response groups (Figure S4). In other experiments, we investigated whether PD-1+ CD8 TEM

frequencies would also stratify subjects by treatment response and found that these cells did not significantly differ over the course of the trials between placebo, R and NR groups. To further refine and characterize the CD8 subsets associated with response, we performed high dimensional CyTOF analysis of activation, differentiation, and exhaustion markers on total CD8 T cells in 12 alefacept-treated subjects, followed by unsupervised clustering and data visualization with Rphenograph and tSNE. Of the 23 clusters defined by RPhenograph, 16 of them contained at least 1% of the total cells and were included in subsequent analyses. Hierarchical clustering of the subsets according to marker intensity revealed the presence of multiple naïve- and memory-like CD8 clusters, including populations expressing high levels of IRs like PD-1, likely corresponding to subsets of the response-associated, IR-high CD8 TEM cells seen by flow cytometry (Figure 2A and Figure 3A).

We compared frequencies of the 16 clusters between response groups over time through the end of the trial (Figure S5). An initial decrease was seen in the frequencies of several memory CD8 clusters across both response groups. For example, cluster 3 (CD25+ CD127+), cluster 1 (KLRG1+ CD161+), and cluster 20 (PD-1+) decreased from baseline to week 35 across subjects. Several naïve CD8 clusters, including cluster 9 (CD127+ CCR7+) and cluster 15 (CD38+ CCR7+), increased in frequency during the same timeframe (Figure 3 and Figure S5). These changes corresponded to the previously described depletion of TEM cells by alefacept and reflected an expected change in population proportions that occurred across all treated subjects in the weeks following therapy (11, 15).

While these broad, post-treatment alterations to the CD8 T cell compartment occurred across subjects regardless of outcome, differences in the frequency changes of two IR-high clusters, clusters 12 and 20, were observed when comparing responders to non-responders (Figure 2B and Figure S5). Although non-responders had significantly more cells in cluster 12 at baseline, the frequency of these cells declined following treatment in non-responders but was maintained at approximately baseline levels in responders over time. Frequency of cells in cluster 20 declined in all subjects following therapy but recovered more

extensively by week 104 in responders than non-responders (Figure 3B). Baseline frequency of cells in cluster 3 (CD45RA+ CD25+) was also associated with response (Figure S5); however, this population declined in both treatment groups and did not significantly differ between them post-treatment. We therefore chose to focus further analyses on clusters 12 and 20 due to their positive correlation with good response, which could indicate a mechanistic role for them in alefacept's efficacy against T1D onset.

Both clusters 12 and 20 expressed CD45RO but not CD45RA, confirming their memory lineage, as well as TIGIT, T-BET, KLRG1, CD244, CD122, and EOMES (Figure 3A and 3C). Although both clusters grouped closely on the tSNE map, forming a large cluster of TEM cells, they could be distinguished from one another by higher expression of CD57 and Granzyme B on Cluster 12 and higher expression of PD-1 on Cluster 20 (Figure 3A). Cluster 20 expressed moderate levels of CD27, which could indicate a transitional memory phenotype.

Cluster 17 expressed high levels of CD57 and GZMB, as well as moderate levels of exhaustion-associated markers TIGIT and CD244 (Figure 3A and Figure S6). However, this cluster also expressed CD45RA and HELIOS, suggesting a more activated, TEMRA-like phenotype inconsistent with functional exhaustion. Cluster 11, another CD45RA- CD45RO+ memory CD8 cluster, expressed low levels of KLRG1 and CD244. However, expression of functional activation markers like HELIOS and CD161 suggests that cluster 11 was not functionally exhausted in spite of moderate expression of IRs and exhaustion-associated transcription factors. Clustering analysis therefore enabled us to distinguish clusters 12 and 20 from other IR-expressing and cytotoxic cells. Cluster 12 appeared to be a subpopulation of the CD57+ and GZMB+ TEM cells characterized by flow cytometry analysis, while Cluster 20 likely corresponded to a PD-1hi subset of the TIGIT+ KLRG1+ TEM population (Figure 2A).

Finally, we correlated the frequencies of clusters 12 and 20 with expression of blue module genes to determine if patterns of gene expression and cell frequencies supported the hypothesis that both the

RNAseq and cytometry response signatures were arising from the same populations of cells (Figure S7 and Figure S8). Positive correlations existed between the blue module gene expression and frequencies of clusters 12 and 20, as well as clusters 3 and 17 (Figure S8). Significant correlations existed between other cluster frequencies and modules (Figure S9); however, the lack of response associations between these modules and clusters led us to focus further analysis on the blue module and clusters 12 and 20.

Although only the correlation with cluster 20 with blue module gene expression reached significance, the trend towards a positive correlation supported the hypothesis that an elevated proportion of these cells likely contributed to the observed elevation in blue module gene expression in responders. However, these positive correlations were not exclusive to clusters 12 and 20. The diverse gene pathways represented in the blue module (Figure 1F) suggested that multiple cell types likely contributed to the total signature, which is supported by the positive correlations between blue module gene expression and frequencies of clusters 3 and 17 in addition to clusters 12 and 20 (Figure S8 and Figure S9).

Together, these results suggest that maintenance of CD8 cells with terminal, exhausted-like phenotypic signatures was linked to better therapy response.

*CD57+ and PD-1+ response-associated CD8 T cells were hypo-proliferative and expressed features of NK function and T cell activation:*

To further characterize the phenotype and function of cells in clusters 12 and 20, we defined these populations as CD8+ CD45RA- PD-1+ (cluster 20) and CD8+ CD45RA- CD57+ (cluster 12) (Figure 4A). Hypergate was used to confirm that these markers were the most likely to yield sorted subsets with the highest possible purity (Figure S10) (35). Sorting only CD45RA- CD8 T cells excluded the naive CD57+ CD45+ population (cluster 17) from the sorted CD57+ population. PD-1 was selected as the primary identity marker for cluster 20 given that its expression was a distinct feature of cluster 20, with only low

expression on a small percentage of cells in cluster 11 and 12 (Fig. 3A and C; Figure S6). The upstream CD8 sort was performed as shown in Figure S2.

To enable comparison with exhausted-like and non-exhausted cells, we also sorted two populations to serve as positive and negative controls for the exhaustion phenotype as previously described (22). These included memory CD8 T cells that co-expressed the IRs TIGIT and KLRG1 (DP) and memory CD8 T cells that expressed neither of these receptors (double negative, or DN). We then performed bulk RNA-sequencing, followed by differential gene expression analysis (DGEA) and rotation gene set testing on the sorted populations.

DGEA revealed higher expression of IRs and exhaustion-associated genes, including *KLRG1*, *TIGIT*, and *EOMES*, in both PD-1+ and CD57+ cells relative to DN cells (Figure 4B). Also relative to DN cells, both PD-1+ and CD57+ cells were enriched for blue module genes, confirming that these cells likely contributed to the gene expression response signature seen in the bulk CD8 RNA-seq analysis (Figure 4C).

To determine the extent to which these populations' gene expression profiles aligned with profiles of DP cells, we defined DP-associated gene set by contrasting our sorted DP and DN cells using limma and selecting genes whose expression was significantly higher in DP relative to DN cells (adjusted $p < 0.05$). We then used this set of DP-associated genes in an enrichment analysis comparing PD-1+ and CD57+ cells with the DN population. Both populations were highly enriched for DP-associated genes relative to DN (Figure S11). These results confirmed that both PD-1+ and CD57+ cells have features associated with exhaustion, consistent with the high IR expression seen on clusters 12 and 20 by CyTOF analysis and elevated DP and CD57+ CD8 TEM cells seen by flow cytometry.

To directly test proliferative activity of PD-1+ and CD57+ cells, we stimulated CD8 memory cell subsets in vitro with anti-CD3 and anti-CD28 monoclonal antibodies (mAbs) and measured Ki67 expression at

day 4 as a measure of proliferation (Figure S12 and Figure 4D). Both PD-1+ and CD57+ subsets were hypoproliferative relative to total memory, PD1-, CD57-, and DN control populations (Figure 4D).

Because CD57 has canonically been used as a marker of senescence, we tested for enrichment of genes related to telomere maintenance, DNA replication, and senescence in the CD57+ relative to PD-1+ cells (Figure S13). We defined a telomere-associated gene set (n=175) derived from overlap between the MSigDB "telomere organization" set and any REACTOME pathways. We also divided these genes into functionally distinct subsets including histones, polymerases, DNA repair, and replication for gene set testing. Enrichment analysis with roast showed that of the total telomere-related gene set and the functional gene sets, only the polymerase genes were significantly enriched in either population, with increased enrichment in PD1+ cells relative to CD57+ cells ($p = 0.01$). Two additional, previously defined gene sets associated with p53 and senescence were also tested for enrichment (36). Both gene sets showed low levels of enrichment in PD-1+ vs CD57+ cells, with one set reaching statistical significance (Figure S14). Together, these results indicated that while the CD57+ cells were hypoproliferative, they did not upregulate genes related to the processes involved in classical senescence.

*CD57+ and PD-1+ TEM cells shared a subset of TCRs but differentially expressed features of NK function and T cell activation:*

To determine if these cells represented two clonally related states of exhaustion, we evaluated TCR sharing to identify potential clonal relationships. We adapted procedures we developed previously for single cell analysis for bulk RNA-seq (37, 38). In preliminary experiments, these procedures were able to accurately detect known, high-abundance re-arranged TRAV and/or TRBV TCR chain CDR3 regions (junctions) in bulk T cell profiles (Materials and Methods). We applied these procedures to our bulk RNA-seq profiles from the sorted PD-1+ and CD57+ cells. Circos plots linking rearranged junctions showed TCR junction

sharing between CD57+ and PD-1+ cells from two of three subjects (Figure 5A). One of these subjects also shared a TCR junction between different visits, suggesting clonotype persistence.

Although there was no junction sharing between the few subjects in this study, we sought to determine if these shared TCRs were public (found in other individuals) or private specificities. Since our bulk profiles do not provide TCR pairing information, we were unable to directly determine antigen specificity of these TCRs. We therefore performed sequence comparisons by BLAST analysis against the NCBI (National Center for Biotechnology) non-redundant protein database (Table S2). We found that rearranged TRAV (TRAV26-2-CILPLAGGTSYGKLTF) and TRBV (TRBV7-8-CASSLGQAYEQYF) chains detected in donor 1 at week 104 perfectly matched a well characterized immunodominant TCR recognizing Epstein Barr Virus (EBV) (39). Using PCR analysis, we found measurable EBV DNA in peripheral blood from this donor at week 104, but not week 52, suggesting that failure to control EBV was associated with likely expansion of exhausted EBV-specific CD8 T cells. Together, our results suggest that the CD57+ and PD-1+ populations shared common precursors in some subjects.

We next directly compared PD-1+ and CD57+ cells by DGEA to distinguish the populations from one another. PD-1+ cells expressed high levels of the genes *CD28*, *IL2*, *CD27* and *PDCD1*, while CD57+ cells expressed higher levels of NK cell receptor (NKRs) genes, including *FCGR3A*, *LILRB1*, *KLRD1*, and multiple Inhibitory Killer cell Immunoglobulin-like Receptor (iKIRs) genes (*KIR2DL1*, *KIR2DL2*, *KIR3DL1*, *KIR3DL2*) (Figure 5B). iKIRs are membrane proteins with inhibitory isoforms that bind HLA class I molecules (40). Signature genes from CD57+ cells comprised a highly interconnected network of genes classically found in NK cells, but also in terminal effector CD8 T cells (41) (Figure 5C).

GO analysis of the genes more highly expressed in CD57+ cells showed enrichment of terms related to NK cell function, as well as cytotoxic functions characteristic to both NK and CD8 T cells (Figure 5D-E**)**. This gene signature suggests functional similarities between the response-associated CD57+ CD8 cells

and NK cells. In contrast, genes more highly expressed in PD-1+ cells were enriched for annotation terms suggesting T cell costimulation (*CD28*, *CD40LG*), proliferation (*IL2*), and differentiation (*IL23A*, *FOXP3*) (Figure 5F-G**)**. Notably, the elevation of these activation-related genes in the PD-1+ cells is relative, and although they appeared to be more active than the CD57+ cells, they had lower expression of activation pathways and reduced proliferative capacity compared to non-naïve and populations with exhausted-like phenotypes (Figure 4).

Finally, to further assess the differences in functional pathways between PD-1+ and CD57+ cells, we compared their enrichment for 111 previously defined gene sets using gene set enrichment analysis (GSEA) (42). Several highly overlapping cytotoxicity-associated modules, including GZMB.mod and CD244.mod, were enriched in CD57+ cells relative to PD-1+ cells. Modules associated with T cell activation, inhibition, and differentiation, such as CD28.mod and CTLA4.mod, were more highly enriched in PD-1+ cells (Figure S15).

## Discussion

Using a combination of transcriptomics, cytometry, and functional assays, we performed a detailed analysis of the phenotype and function of residual and recurrent CD8 T cells following alefacept therapy in RO T1D subjects. This systems level approach identified a response-associated CD8 T cell signature that was defined by activation and exhaustion-associated gene expression and higher frequency of two related, but unique, CD8 memory phenotypes. These IR-expressing cells expressed features of exhaustion but were phenotypically distinct from one another, distinguishable by high reciprocal expression of PD-1 or CD57. The divergent inhibitory phenotypes of these cells, including iNKR expression by the CD57+ cells, point to a possible role for multiple inhibitory systems driving effector CD8 T cells towards an inhibited or exhausted state that could be beneficial in the context of T1D and other autoimmune diseases.

We showed that the sorted CD57+ and PD-1+ cells shared some rearranged TCR sequences, a commonly used measure of T cell clonality. This finding suggests that CD57+ and PD-1+ cells shared a common lineage. However, because of the limited scope of our observations, we are unable to discriminate between different models for how CD57+ and PD-1+ cells are derived from a common ancestral precursor. Larger studies utilizing single cell RNA-seq and samples taken over time will be required to clarify these lineage relationships. Such studies may also clarify TCR pairing and antigen specificity of exhausted cells. Integrating knowledge of lineage relationships and antigen specificity will permit a fuller understanding of the relationship of exhausted cells in T1D progression and response to therapy.

The hypoproliferative DP cells described in the AbATE trial (22, 43) were defined by their expression of the transcription factor EOMES, effector molecules, and multiple IRs, including TIGIT and KLRG1, and were found to expand after treatment. The subtypes of CD8 T cells associated with response to alefacept, however, were distinct from these DP cells. First, the population dynamics differed in that clusters 12 and 20 did not expand from baseline frequencies, but rather were maintained or recovered to baseline levels

after treatment in responders as compared to non-responders. Therefore, while both drugs may induce or spare a favorable, tolerogenic CD8 T cell phenotype, the dynamics of these cells may reflect differences in drug mechanisms. Teplizumab targets CD3, and as an agonist of the receptor could activate cells and thereby induce exhaustion. In contrast, alefacept targets CD2hi cells and therefore depletes activated effector memory subsets. It is possible that alefacept also acts by inhibiting costimulation by blocking CD2 signaling, thereby inducing functional inhibition rather than depletion (15). TREGs were also spared, so this combined with functional inhibition of effector cells may have promoted a more tolerogenic immune state in alefacept responders. We note, however, that we have not detected TREG signatures in either previous (22, 24) or the present studies of biologic therapies in T1D.

The CD57+ cells expressed features of cytotoxicity not seen in canonically exhausted cells. Expression of CD57 on the surface of CD8+ T cells increases during T cell differentiation and is considered a marker of cytotoxic function (44-46). CD57 is expressed by heterogeneous populations of memory T cells and terminally differentiated effector T cells (45-47). CD57+ CD8 T cells have been described as senescent in chronic HIV infection (47), and in other diseases with chronic immune stimulation such as rheumatoid arthritis and in transplantation (44-46). During chronic viral infections, senescent T cells express CD57, KLRG1, and killer-cell immune globulin-like receptors and are capable of producing significant amount of effector cytokines (48). In T1D, elevated expression of CD57 and CD95 has been described in β-islet cell-specific CD8 T cells of patients with newly diagnosed type 1 diabetes compared to healthy controls, and these cells are present in subjects with higher levels of C-peptide (49), raising the possibility that these cells participate in a protective, rather than pathogenic, role. In a follow up study, the same group showed that change in β cell-specific effector memory CD8+ T cells expressing CD57 was positively correlated with C-peptide change in subjects below 12 years of age. Autoreactive CD57+ effector memory CD8+ T cells bore the signature of enhanced effector function (higher expression of Granzyme B, killer-specific protein of 37 kDa, and

CD16, and reduced expression of CD28) compared with their CD57- counterparts, and network association modeling indicated that the dynamics of β cell-reactive CD57+ effector memory CD8+ T cell subsets were strongly linked (50). These results suggest that cytotoxic, CD57+ CD8 TEM cells may play a protective role during the early stages of T1D and in subjects who maintain higher C-peptide over time. However, they have not been identified in all subjects with high or maintained levels of C-peptide (26).

Alternatively, the protective effect of CD57+ CD8 T cells observed here and in previous trials could reflect the loss of cytotoxic function in a subset of terminal, cytotoxic CD57+ cells. Increased expression of inhibitory receptors, including iNKRs, concurrent with a reduction in activation markers like CD28 and HELIOS, as well as loss of proliferative capacity, could be indicative of the expansion or maintenance of a dysfunctional, exhausted-like CD57+ CD8 T cell subset in subjects with better outcomes in T1D. Our observation of multiple phenotypically distinct CD57+ clusters by CyTOF analysis (Figure 3A) suggests that CD57 marks multiple functionally discrete cell types spanning a range of functional ability, and that cytotoxic function itself may not be the protective mechanism at play in this and other trials.

The higher frequency of cluster 12 in non-responders at baseline may suggest that a higher frequency of CD57+ exhausted-like CD8 T cells is predictive of a negative outcome. Alternatively, the consistent frequency of cluster 12 in responders over time suggests that maintenance of a small terminal CD57+ population, as opposed to the depletion of it, may be beneficial to therapy response and outcome. A beneficial role for CD57+ CD8 T cells is also supported by the manual gating analysis of GZMB+ and CD57+ CD8 T cells (Figure 2) that showed a slight increase in the frequencies of these populations over time in responders versus non-responders.

Although it is not evident why non-responders underwent depletion of cluster 12 cells and responders did not, it is possible that these cells expressed higher levels of CD2 in non-responders than in responders,

making the cells more prone to depletion by alefacept. The maintenance of gated CD57+ and GZMB+ TEM cells in placebo-treated subjects (Figure 2) suggests that the reduction seen in these populations is specific to alefacept treatment as opposed to natural disease progression. Further experimentation is needed to clarify the phenotypic or functional differences that might have contributed to differential depletion of cluster 12 cells between response groups in this trial.

Recent studies have identified subtypes of TEX cells defined by their differentiation state and proliferative and functional ability. Precursor exhausted cells retain their proliferative potential, whereas terminally exhausted cells have lost their ability to divide as well as all functional capability. In addition to loss of function and proliferative capacity, the trajectory from a precursor to terminally exhausted state is characterized by changes in surface marker and transcription factor expression, including increased expression of PD-1 and decreased expression of activation receptors. The PD-1+ cells defined here resembles the stem-like (51), precursor (52) or progenitor (53) exhausted cells identified by others, in that they are hypoproliferative, PD-1 high, but appear to retain some activation-associated functions. The CD57+ cells defined here, however, does not clearly fall along previously described trajectories, as neither CD57 nor iKIRs are present in T or NK cells in mice (54), where much of the fundamental work on exhaustion has been done. The expression of cytotoxic markers by CD57+iKIR+ cells may indicate that they represent a distinct lineage of exhausted-like cells.

PD-1/PD-L1 ligation inhibits TCR signaling by preferentially dephosphorylating CD28 (55, 56). The PD-1+ cells in this study maintained a high level of CD28 gene expression and thus would be expected to remain sensitive to inhibition by PD-1/PD-L1 signaling. In contrast, upregulation of iKIRs on the CD57+ CD28- cells could reflect an alternative, CD28-independent inhibitory mechanism. In other studies, upregulation of NKRs, including iKIRs, was observed in CD8 T cells following loss of CD28, and these receptors were shown to provide a costimulatory signal to prolong CD8 T cell survival and function (41). The CD57+ cells described here could represent a terminally exhausted phenotype deriving directly from

391 the PD-1+ cells after they have lost CD28 expression. The functional consequences of these CD57+, "post-
392 exhaustion" cells on disease and outcome could be determined by the quality (i.e. inhibitory or activating)
393 of NKR upregulation that occurs following loss of CD28. Inhibitory KIR expression, as observed here,
394 would contribute to an inhibitory and thus potentially protective immune state for autoimmune disease.

395 The reciprocal expression pattern of *PDCD1* and iKIRs in CD8 T cells has been noted previously.
396 Duraiswamy et al. (57) described the striking observation that KIRs and killer cell lectin-like receptor
397 (KLRs) were completely downregulated on PD1hi cells. Boelen et al. (58) discussed similarities between
398 the iKIR-HLA receptor-ligand system and the PD1–programmed death ligand 1/2 system. Both iKIR and
399 PD-1 are inhibitory receptors that block proximal TCR signaling and are up-regulated in the context of
400 chronic viral infection and on tumor-infiltrating lymphocytes. Our results support these previous studies
401 and extend them into the realm of therapies for T1D, and perhaps other autoimmune diseases.

402 iKIRs can affect T cell responses indirectly through NK cells or directly via expression on CD8+ T cells
403 (58). Recent evidence shows that functional engagement of iKIRs by their MHC ligands enhances clinical
404 CD8+ T cell responses against HIV-1, HCV, and HTLV-1 viral infections (58). Other studies have shown
405 a role for KIRs and IRs in EBV infections, such that in later stages of persistent infection, protective
406 immunity to EBV may be reduced due to the preferential accumulation of hyporesponsive EBV-specific
407 CD8+ T cells (59). These findings are consistent with our demonstration of expanded EBV-specific TCRs
408 in CD57+ CD8 cells, although in autoimmunity, hypo-responsiveness is clinically beneficial. It is
409 important to note that our observations were made at the transcriptome level and that a fuller understanding
410 of the functional implications of iKIRS in autoimmune disease progression will require additional
411 experimentation with the protein products of these genes.

412 The statistical comparisons in this study were limited by small sample sizes, particularly in the analysis
413 of discretized response (responder/non-responder) where only 6-9 subjects were available per group at

post-treatment time points. Future studies would benefit from a larger sample size to confirm and further characterize the role of exhausted or exhausted-like CD8 T cells in T1D immunotherapy response.

Taken together, these studies support an association between IR-expression, hypoproliferative CD8 T cells and favorable outcome in T1D trials of immunomodulatory agents, although the mechanisms and molecular targets of initial immune perturbation differ with each agent used. This study also provides evidence that inhibitory NKR expression on hypoproliferative CD8 T cells may be protective against the autoimmune response in T1D. Alefacept and other T1D therapies may therefore drive self-reactive T cells to a more exhausted state by promoting one or more differentiation pathways, thereby preventing further beta cell destruction.

## Methods

### Study design and patients

T1DAL was a phase-2, randomized, placebo controlled, double-blind clinical trial conducted at 14 clinical centers in the United States with a 9-month treatment period and 15 months of follow-up. Eligible participants were 12–35 years of age at the time of screening; <100 days from diagnosis at the time of enrollment; positive for at least one diabetes-associated autoantibody (insulin, GAD-65, IA-2, ZnT8, or ICA); and had peak-stimulated C-peptide of >0.2 nmol/L during a MMTT (11, 15). All subjects gave informed consent prior to enrollment in the trial. Eligible subjects were randomly assigned 2:1 to alefacept (33 patients) or placebo (16 patients). Participants received 15 mg alefacept (Amevive, Astellas) or equivalent volume of saline (placebo) i.m. weekly for 12 weeks and, after a 12-week pause, 12 additional weekly doses of alefacept or placebo. Participants underwent a 4-hour MMTT at screening, 52 weeks, and 104 weeks; a 2-hour MMTT at 24 and 78 weeks; and intensive diabetes management. Additional participant and outcome data from the T1DAL trial are available online at (https://www.itntrialshare.org/T1DAL.url). Peripheral blood mononuclear cells (PBMC) were collected

from 30 alefacept-treated and 12 Placebo-treated patients at weeks 0, 11, 24, 35, 52, 78, and 104 for flow cytometry and at weeks 0, 24, 35, 52, and 104 for RNAseq and CyTOF (Figure 1A), followed by functional studies on selected samples. Responders were defined as participants that maintained or increased their baseline 4-hour C-peptide AUC (n=9). Non-responders were defined as participants that had greater than 40% loss of their 4-hour baseline C-peptide AUC values at 2 years (n=9), consistent with prior ITN studies (15, 60).

**Flow cytometry immunophenotyping**

Flow cytometry analysis was run on 39 subjects (R=7, NR=9, PR=11, and P=12) from 7 visits (weeks 0, 11, 24, 35, 52, 78, and 104). Cryopreserved PBMCs from all subjects were thawed, incubated with FcX Block and stained with X-trial T and NK cell flow cytometry panels used in previously reported ITN studies (22, 43, 61) (Table S3). Instrument standardization was performed using 8 peak rainbow calibration beads (Spherotech, Lake Forest, IL) adjusting PMT voltages for consistent $7^{th}$ peak mean fluorescent intensities. All samples from the same subject were run on the same day, and an internal control arm from the same subject was run each week. An average of 580,000 live lymphocyte events were collected per sample on a BD Fortessa using Diva software and data was analyzed using Flowjo Mac Version 9.4 (Tree Star Inc., Ashland, OR). Gated populations with <100 events were excluded from analysis.

**T cell proliferation assay**

Cryopreserved PBMCs from 4 Alefacept treated subjects at weeks 52 or 104 were thawed and sorted into non naïve (CD45RA-), PD1+ and KLRG1+TIGIT+ non-naïve CD8 T cells and labelled with cell trace violet (ThermoFIsher). The labelled cells were mixed back with unlabeled autologous PBMC and stimulated in vitro with plate bound anti-CD3 and anti-CD28 monoclonal antibodies for three days. Proliferation was measured by Ki67 expression within all CD8 populations. Representative plots

for CD8 populations and the gating strategy for Ki67 are shown in Figure S12. The staining panels for sorting and proliferation are shown in Tables S4 and S5. Flow acquisition and analysis was performed as described above.

**RNA-seq**

Out of 33 treated alefacept-treated subjects, 3 were lost to follow-up by week 104. Samples from the remaining 30 treated subjects (weeks 0, 24, 35, 52, and 104) were analyzed by RNA-sequencing. Bulk CD8 T cells were FACS-sorted and analyzed by RNA-seq as previously described (22). Low quality libraries (median CV of coverage > 0.9, total reads < 5 million) were excluded, leaving 26 subjects with libraries available from downstream analysis (see Table S1). Counts were then normalized and log2-transformed, followed by batch correction using the limma R package (62). Five placebo subjects were included in the week 104 RNA-seq analysis, and the 3 placebo samples that remained after QC filtering were included in the WGCNA analysis to maximize the sample size for module detection. The top 5000 most variable genes (ranked by coefficient of variation) were used to generate WGCNA modules using the *blockwiseModules* function from the WGCNA R package (34, 63). Weighted gene co-expression network analysis (WGCNA) was run with a soft thresholding power of 5, a signed network, minimum module size of 50, and clustering dendrogram cut height of 0.30. Module eigengenes were calculated using the *moduleEigengenes* function in the WGCNA R package (34, 63), and Pearson's correlation was calculated between these eigengenes and other parameters including clinical outcomes, CyTOF marker levels, and CyTOF cluster frequencies. Gene ontology analysis was performed using the *goana* function in the limma R package (62). String-db (https://string-db.org/) was used to find connected gene networks, and Cytoscape was used to for gene network visualization (64).

Sequences of rearranged TCR chains, which include non-templated nucleotides in the CDR3 junction, not present in the reference genome, were identified from genome-independent (de novo) assemblies of overlapping DNA segments (38, 65). Pilot spike-in experiments showed that rearranged TCRs could be reassembled from high abundance clonotypes in bulk RNA-seq T cell profiles, but not from monocyte profiles.

**Mass cytometry (CyTOF) staining and analysis**

Thawed cryopreserved PBMC were stained for viability using cisplatin (Enzo Life Sciences) prior to staining with a surface antibody cocktail (Table S6). Samples were then washed, fixed using the Maxpar Nuclear Antigen Staining Buffer (Fluidigm), and stained with an intracellular mAb cocktail. Samples were stored with 125 nM MaxPar Intercalator-Ir (Fluidigm) in Fix and Perm Buffer (Fluidigm) at 4$^{o}$C over night or up to 1 week prior to acquisition. For acquisition, cells were resuspended ($0.5x10^{6}$/mL) in cold ultrapure water containing 1/5$^{th}$ EQ Four Element Calibration Beads (Fluidigm) and were acquired at a rate of 300-500 events/second on a CyTOF1.5 with upgrades (Fluidigm) running CyTOF Sofware version 6.0.626 and using a Super Sampler system (Victorian Airship & Scientific Apparatus). Files were converted to .FCS and then randomized and normalized for EQ bead intensity using the CyTOF Software. FlowJo software (version 10.4) was used to manually gate and export FCS files of $CD8^{+}$ T cells.

Gated CD8 T cells were analyzed in R using the Cytofkit and flowCore packages (66). Events were down-sampled to include the same number of events from each subject at each time point, and were then combined for all downstream analyses. Intensity values were arcsinh-transformed with a cofactor of 5 prior to analysis. Markers that were used for preliminary gating and those with a high CV were excluded from dimensionality reduction and clustering. The full set of markers used to generate t-SNE plots and clusters was: CCR7, CD38, CXCR3, CD27, CD45RA, CD45RO, CD57, CD25, TIGIT, EOMES, T-BET,

CD95, HELIOS, KLRG1, TIM3, PD1, CD122, 24B, CD161, CD127, and NKG2D. Rphenograph (67) was used to generate clusters from down-sampled files.

**Statistical analysis**

Longitudinal flow cytometry and RNA-seq data were analyzed by repeated measures one-way ANOVA. Group comparisons were made by comparing their least square means at each visit. Mann-Whitney U test was used for comparison between two distinct groups, and within group comparisons were performed by Wilcoxon test. C-peptide slopes were calculated by fitting a random effects linear model over all visits per subject as previously described (68).

Group comparisons of C-peptide data at primary endpoint were analyzed by fitting an ANCOVA model with change from baseline as the outcome and baseline value as a covariate. False discover rate (FDR) or Bonferroni correction were applied where appropriate to adjust for multiple comparisons for statistical tests. All comparisons required the level of significance to be kept at $\alpha$ of 0.05 for two-sided tests. SAS version 9.4 was used for all data analyses, and graphs were produced in R (https://www.R-project.org). Datasets for these analyses are accessible through TrialShare, a public website managed by the ITN (https://www.itntrialshare.org/T1DAL.url), and the GEO Repository, accession GSE158292. Code and data files used in figures are deposited at GitHub (https://github.com/BenaroyaResearch/Diggins_Serti_Linsley_JCI_Insight_2020; commit ID 918a8972f9a87842a4385966491320a9f5afd184).

To determine correlations between gene expression and the frequency (percentage) of specific cell types identified by CyTOF, Pearson's correlation values were calculated between blue module eigengene values and cell type frequencies from Rphenograph. Student's asymptotic two-tailed t test was then used to calculate the significance of the correlations. A P value less than 0.05 was considered significant.

Error bars indicate mean ± SEM.

## Study approval

The T1DAL study was approved by independent institutional review boards at each participating clinical center. All participants or parents provided written informed consent or assent (<18 years old) (15).

**Author contributions**: K.E.D. and E.S. performed experiment design, data analysis, figure generation, and writing. V.M. assisted with data analysis and manuscript edits. M. R. assisted with data analysis. T.L. performed statistical analysis, figure generation, and data management, and acted as consulting statistician. E.B. assisted with data analysis. G.N. provided guidance on experiment design, figure design, and data management. S.A.L. and P.S.L contributed to experiment design and execution, data analysis, data management, and writing. **Competing interests**: Astellas provided alefacept (Amevive) for the T1DAL clinical trial and gave input regarding dosage and safety, but had no involvement with the study design, conduct, analysis, or manuscript preparation of this report.

**Acknowledgments:** The authors would like to thank Philip Bernstein, Kristina Harris and Srinath Sanda for reviewing data and providing feedback; Jorge Pardo for flow cytometry analysis; Alice E. Wiedeman, Valerie Wall and Bryce Fuchs for performing experiments; Matt Dufort for statistical analysis; Olivia Doyle for experiment coordination; Carol Soppe for trial coordination; Cate Speake and Carla Greenbaum for providing samples and insightful discussions; and the BRI HIP Core for performing the longitudinal flow cytometry acquisition and analysis. **Funding**: This study was conducted by the ITN and sponsored by the National Institute of Allergy and Infectious Diseases (NIAID) under Award UM1AI109565. Additional funding was provided by the National Institute of Diabetes and Digestive and Kidney Diseases (NIDDK). This report is solely the responsibility of the authors and does not necessarily represent the official views of the NIH.

552 References

553


554 1. Bluestone JA, Herold K, and Eisenbarth G. Genetics, pathogenesis and clinical interventions in
555 type 1 diabetes. *Nature.* 2010;464(7293):1293-300.
556 2. Bougneres PF, Carel JC, Castano L, Boitard C, Gardin JP, Landais P, et al. Factors associated with
557 early remission of type I diabetes in children treated with cyclosporine. *N Engl J Med.*
558 1988;318(11):663-70.
559 3. Castano L, Boitard C, and Bougneres PF. Cyclosporin A suppresses insulin autoantibodies and
560 heterologous insulin antibodies in type I diabetic children. *Diabetes.* 1988;37(8):1049-52.
561 4. Herold KC, Hagopian W, Auger JA, Poumian-Ruiz E, Taylor L, Donaldson D, et al. Anti-CD3
562 monoclonal antibody in new-onset type 1 diabetes mellitus. *N Engl J Med.* 2002;346(22):1692-8.
563 5. Keymeulen B, Vandemeulebroucke E, Ziegler AG, Mathieu C, Kaufman L, Hale G, et al. Insulin
564 needs after CD3-antibody therapy in new-onset type 1 diabetes. *N Engl J Med.* 2005;352(25):2598-
565 608.
566 6. Pescovitz MD, Greenbaum CJ, Krause-Steinrauf H, Becker DJ, Gitelman SE, Goland R, et al.
567 Rituximab, B-lymphocyte depletion, and preservation of beta-cell function. *N Engl J Med.*
568 2009;361(22):2143-52.
569 7. Sherry N, Hagopian W, Ludvigsson J, Jain SM, Wahlen J, Ferry RJ, Jr., et al. Teplizumab for
570 treatment of type 1 diabetes (Protege study): 1-year results from a randomised, placebo-controlled
571 trial. *Lancet.* 2011;378(9790):487-97.
572 8. Long SA, Rieck M, Sanda S, Bollyky JB, Samuels PL, Goland R, et al. Rapamycin/IL-2
573 combination therapy in patients with type 1 diabetes augments Tregs yet transiently impairs beta-
574 cell function. *Diabetes.* 2012;61(9):2340-8.
575 9. Hagopian W, Ferry RJ, Jr., Sherry N, Carlin D, Bonvini E, Johnson S, et al. Teplizumab preserves
576 C-peptide in recent-onset type 1 diabetes: two-year results from the randomized, placebo-
577 controlled Protege trial. *Diabetes.* 2013;62(11):3901-8.
578 10. Herold KC, Gitelman SE, Ehlers MR, Gottlieb PA, Greenbaum CJ, Hagopian W, et al. Teplizumab
579 (anti-CD3 mAb) treatment preserves C-peptide responses in patients with new-onset type 1
580 diabetes in a randomized controlled trial: metabolic and immunologic features at baseline identify
581 a subgroup of responders. *Diabetes.* 2013;62(11):3766-74.
582 11. Rigby MR, DiMeglio LA, Rendell MS, Felner EI, Dostou JM, Gitelman SE, et al. Targeting of
583 memory T cells with alefacept in new-onset type 1 diabetes (T1DAL study): 12 month results of
584 a randomised, double-blind, placebo-controlled phase 2 trial. *Lancet Diabetes Endocrinol.*
585 2013;1(4):284-94.
586 12. Pescovitz MD, Greenbaum CJ, Bundy B, Becker DJ, Gitelman SE, Goland R, et al. B-lymphocyte
587 depletion with rituximab and beta-cell function: two-year results. *Diabetes Care.* 2014;37(2):453-
588 9.
589 13. Bluestone JA, Buckner JH, Fitch M, Gitelman SE, Gupta S, Hellerstein MK, et al. Type 1 diabetes
590 immunotherapy using polyclonal regulatory T cells. *Sci Transl Med.* 2015;7(315):315ra189.
591 14. Haller MJ, Gitelman SE, Gottlieb PA, Michels AW, Rosenthal SM, Shuster JJ, et al. Anti-
592 thymocyte globulin/G-CSF treatment preserves beta cell function in patients with established type
593 1 diabetes. *J Clin Invest.* 2015;125(1):448-55.
594 15. Rigby MR, Harris KM, Pinckney A, DiMeglio LA, Rendell MS, Felner EI, et al. Alefacept
595 provides sustained clinical and immunological effects in new-onset type 1 diabetes patients. *J Clin*
596 *Invest.* 2015;125(8):3285-96.
597 16. Gitelman SE, and Bluestone JA. Regulatory T cell therapy for type 1 diabetes: May the force be
598 with you. *J Autoimmun.* 2016;71:78-87.

17. Gitelman SE, Gottlieb PA, Felner EI, Willi SM, Fisher LK, Moran A, et al. Antithymocyte globulin therapy for patients with recent-onset type 1 diabetes: 2 year results of a randomised trial. *Diabetologia.* 2016;59(6):1153-61.
18. Haller MJ, Gitelman SE, Gottlieb PA, Michels AW, Perry DJ, Schultz AR, et al. Antithymocyte Globulin Plus G-CSF Combination Therapy Leads to Sustained Immunomodulatory and Metabolic Effects in a Subset of Responders With Established Type 1 Diabetes. *Diabetes.* 2016;65(12):3765-75.
19. Haller MJ, Schatz DA, Skyler JS, Krischer JP, Bundy BN, Miller JL, et al. Low-Dose Anti-Thymocyte Globulin (ATG) Preserves beta-Cell Function and Improves HbA1c in New-Onset Type 1 Diabetes. *Diabetes Care.* 2018;41(9):1917-25.
20. McKinney EF, Lee JC, Jayne DR, Lyons PA, and Smith KG. T-cell exhaustion, co-stimulation and clinical outcome in autoimmunity and infection. *Nature.* 2015;523(7562):612-6.
21. Herold KC, Bundy BN, Long SA, Bluestone JA, DiMeglio LA, Dufort MJ, et al. An Anti-CD3 Antibody, Teplizumab, in Relatives at Risk for Type 1 Diabetes. *N Engl J Med.* 2019;381(7):603-13.
22. Long SA, Thorpe J, DeBerg HA, Gersuk V, Eddy J, Harris KM, et al. Partial exhaustion of CD8 T cells and clinical response to teplizumab in new-onset type 1 diabetes. *Sci Immunol.* 2016;1(5).
23. Linsley PS, Greenbaum CJ, Speake C, Long SA, and Dufort MJ. B lymphocyte alterations accompany abatacept resistance in new-onset type 1 diabetes. *JCI insight.* 2019;4(4):e126136.
24. Linsley PS, Greenbaum CJ, Rosasco M, Presnell S, Herold KC, and Dufort MJ. Elevated T cell levels in peripheral blood predict poor clinical response following rituximab treatment in new-onset type 1 diabetes. *Genes Immun.* 2019;20(4):293-307.
25. Dufort MJ, Greenbaum CJ, Speake C, and Linsley PS. Cell type-specific immune phenotypes predict loss of insulin secretion in new-onset type 1 diabetes. *JCI insight.* 2019;4(4):e125556.
26. Wiedeman AE, Muir VS, Rosasco MG, DeBerg HA, Presnell S, Haas B, et al. Autoreactive CD8+ T cell exhaustion distinguishes subjects with slow type 1 diabetes progression. *The Journal of clinical investigation.* 2020;130(1):480-90.
27. Chaarani J, and Lebwohl M. Alefacept: where it stands today. *Expert Opin Drug Metab Toxicol.* 2010;6(3):355-61.
28. Majeau GR, Meier W, Jimmo B, Kioussis D, and Hochman PS. Mechanism of lymphocyte function-associated molecule 3-Ig fusion proteins inhibition of T cell responses. Structure/function analysis in vitro and in human CD2 transgenic mice. *J Immunol.* 1994;152(6):2753-67.
29. Ellis CN, Krueger GG, and Alefacept Clinical Study G. Treatment of chronic plaque psoriasis by selective targeting of memory effector T lymphocytes. *N Engl J Med.* 2001;345(4):248-55.
30. Krueger GG. Selective targeting of T cell subsets: focus on alefacept - a remittive therapy for psoriasis. *Expert Opin Biol Ther.* 2002;2(4):431-41.
31. Cooper JC, Morgan G, Harding S, Subramanyam M, Majeau GR, Moulder K, et al. Alefacept selectively promotes NK cell-mediated deletion of CD45R0+ human T cells. *Eur J Immunol.* 2003;33(3):666-75.
32. Chamian F, Lowes MA, Lin SL, Lee E, Kikuchi T, Gilleaudeau P, et al. Alefacept reduces infiltrating T cells, activated dendritic cells, and inflammatory genes in psoriasis vulgaris. *Proc Natl Acad Sci U S A.* 2005;102(6):2075-80.
33. Haider AS, Lowes MA, Gardner H, Bandaru R, Darabi K, Chamian F, et al. Novel Insight into the Agonistic Mechanism of Alefacept In Vivo: Differentially Expressed Genes May Serve as Biomarkers of Response in Psoriasis Patients. 2007;178(11):7442-9.
34. Langfelder P, and Horvath S. WGCNA: an R package for weighted correlation network analysis. *BMC Bioinformatics.* 2008;9:559.

35. Becht E, Simoni Y, Coustan-Smith E, Evrard M, Cheng Y, Ng LG, et al. Reverse-engineering flow-cytometry gating strategies for phenotypic labelling and high-performance cell sorting. *Bioinformatics.* 2019;35(2):301-8.
36. Fischer M. Census and evaluation of p53 target genes. *Oncogene.* 2017;36(28):3943-56.
37. Cerosaletti K, Barahmand-pour-Whitman F, Yang J, DeBerg HA, Dufort MJ, Murray SA, et al. Single-Cell RNA Sequencing Reveals Expanded Clones of Islet Antigen-Reactive CD4<sup>+</sup> T Cells in Peripheral Blood of Subjects with Type 1 Diabetes. *The Journal of Immunology.* 2017;199(1):323-35.
38. Bolotin DA, Poslavsky S, Mitrophanov I, Shugay M, Mamedov IZ, Putintseva EV, et al. MiXCR: software for comprehensive adaptive immunity profiling. *Nature Methods.* 2015;12(5):380-1.
39. Kjer-Nielsen L, Clements CS, Brooks AG, Purcell AW, McCluskey J, and Rossjohn J. The 1.5 A crystal structure of a highly selected antiviral T cell receptor provides evidence for a structural basis of immunodominance. *Structure.* 2002;10(11):1521-32.
40. Parham P, and Guethlein LA. Genetics of Natural Killer Cells in Human Health, Disease, and Survival. *Annual Review of Immunology.* 2018;36(1):519-48.
41. Seyda M, Elkhal A, Quante M, Falk CS, and Tullius SG. T Cells Going Innate. *Trends Immunol.* 2016;37(8):546-56.
42. Linsley PS, Chaussabel D, and Speake C. The Relationship of Immune Cell Signatures to Patient Survival Varies within and between Tumor Types. *PLoS One.* 2015;10(9):e0138726.
43. Long SA, Thorpe J, Herold KC, Ehlers M, Sanda S, Lim N, et al. Remodeling T cell compartments during anti-CD3 immunotherapy of type 1 diabetes. *Cell Immunol.* 2017;319:3-9.
44. Wang EC, Lawson TM, Vedhara K, Moss PA, Lehner PJ, and Borysiewicz LK. CD8high+ (CD57+) T cells in patients with rheumatoid arthritis. *Arthritis Rheum.* 1997;40(2):237-48.
45. Rowbottom AW, Garland RJ, Lepper MW, Kaneria SS, Goulden NJ, Oakhill A, et al. Functional analysis of the CD8+CD57+ cell population in normal healthy individuals and matched unrelated T-cell-depleted bone marrow transplant recipients. *Br J Haematol.* 2000;110(2):315-21.
46. Sze DM, Giesajtis G, Brown RD, Raitakari M, Gibson J, Ho J, et al. Clonal cytotoxic T cells are expanded in myeloma and reside in the CD8(+)CD57(+)CD28(-) compartment. *Blood.* 2001;98(9):2817-27.
47. Brenchley JM, Karandikar NJ, Betts MR, Ambrozak DR, Hill BJ, Crotty LE, et al. Expression of CD57 defines replicative senescence and antigen-induced apoptotic death of CD8+ T cells. *Blood.* 2003;101(7):2711-20.
48. Schurich A, and Henson SM. The Many Unknowns Concerning the Bioenergetics of Exhaustion and Senescence during Chronic Viral Infection. *Front Immunol.* 2014;5:468.
49. Skowera A, Ladell K, McLaren JE, Dolton G, Matthews KK, Gostick E, et al. beta-cell-specific CD8 T cell phenotype in type 1 diabetes reflects chronic autoantigen exposure. *Diabetes.* 2015;64(3):916-25.
50. Yeo L, Woodwyk A, Sood S, Lorenc A, Eichmann M, Pujol-Autonell I, et al. Autoreactive T effector memory differentiation mirrors beta cell function in type 1 diabetes. *J Clin Invest.* 2018;128(8):3460-74.
51. Hudson WH, Gensheimer J, Hashimoto M, Wieland A, Valanparambil RM, Li P, et al. Proliferating Transitory T Cells with an Effector-like Transcriptional Signature Emerge from PD-1+ Stem-like CD8+ T Cells during Chronic Infection. *Immunity.* 2019;51(6):1043-58.e4.
52. Chen Z, Ji Z, Ngiow SF, Manne S, Cai Z, Huang AC, et al. TCF-1-Centered Transcriptional Network Drives an Effector versus Exhausted CD8 T Cell-Fate Decision. *Immunity.* 2019;51(5):840-55.e5.
53. Miller BC, Sen DR, Al Abosy R, Bi K, Virkud YV, LaFleur MW, et al. Subsets of exhausted CD8+ T cells differentially mediate tumor control and respond to checkpoint blockade. *Nature Immunology.* 2019;20(3):326-36.

54. Mestas J, and Hughes CCW. Of mice and not men: differences between mouse and human immunology. *Journal of immunology (Baltimore, Md : 1950).* 2004;172(5):2731-8.
55. Hui E, Cheung J, Zhu J, Su X, Taylor MJ, Wallweber HA, et al. T cell costimulatory receptor CD28 is a primary target for PD-1-mediated inhibition. *Science.* 2017;355(6332):1428-33.
56. Kamphorst AO, Wieland A, Nasti T, Yang S, Zhang R, Barber DL, et al. Rescue of exhausted CD8 T cells by PD-1-targeted therapies is CD28-dependent. *Science.* 2017;355(6332):1423-7.
57. Duraiswamy J, Ibegbu CC, Masopust D, Miller JD, Araki K, Doho GH, et al. Phenotype, Function, and Gene Expression Profiles of Programmed Death-1<sup>hi</sup> CD8 T Cells in Healthy Human Adults. *The Journal of Immunology.* 2011;186(7):4200-12.
58. Boelen L, Debebe B, Silveira M, Salam A, Makinde J, Roberts Ch, et al. Inhibitory killer cell immunoglobulin-like receptors strengthen CD8<sup>+</sup> T cell–mediated control of HIV-1, HCV, and HTLV-1. *Science Immunology.* 2018;3(29):eaao2892.
59. Poon K, Montamat-Sicotte D, Cumberbatch N, McMichael AJ, and Callan MFC. Expression of leukocyte immunoglobulin-like receptors and natural killer receptors on virus-specific CD8+ T cells during the evolution of Epstein-Barr virus-specific immune responses in vivo. *Viral Immunol.* 2005;18(3):513-22.
60. Tooley JE, Vudattu N, Choi J, Cotsapas C, Devine L, Raddassi K, et al. Changes in T-cell subsets identify responders to FcR-nonbinding anti-CD3 mAb (teplizumab) in patients with type 1 diabetes. *Eur J Immunol.* 2016;46(1):230-41.
61. B. Burrell SF, N. Bridges, U. Ekong, S. Kanaparthi, A. Kirk, A. Long, K. Spain, L. Stempora, L. Turka, N. Tchao. . Tolerant Pediatric Liver Transplant (LT) Recipients (TOL) from WISP-R (NCT00320606) Split into Two Phenotypically Distinct Groups by PD1 Expression on CD4+ T Cells at Baseline, Prior to Immunosuppression Withdrawal (ISW). . *Am J Transplant.* 2017;17(Suppl 3):American Transplant Congress, Chicago, IL, April 29 – May 3. .
62. Ritchie ME, Phipson B, Wu D, Hu Y, Law CW, Shi W, et al. limma powers differential expression analyses for RNA-sequencing and microarray studies. *Nucleic Acids Res.* 2015;43(7):e47.
63. Langfelder P, and Horvath S. Fast R Functions for Robust Correlations and Hierarchical Clustering. *J Stat Softw.* 2012;46(11).
64. Shannon P MA, Ozier O, Baliga NS, Wang JT, Ramage D, Amin N, Schwikowski B, Ideker T. Cytoscape: a software environment for integrated models of biomolecular interaction networks. *Genome Research.* 2003;13(11).
65. Grabherr MG, Haas BJ, Yassour M, Levin JZ, Thompson DA, Amit I, et al. Full-length transcriptome assembly from RNA-Seq data without a reference genome. *Nature Biotechnology.* 2011;29(7):644-52.
66. Chen H, Lau MC, Wong MT, Newell EW, Poidinger M, and Chen J. Cytofkit: A Bioconductor Package for an Integrated Mass Cytometry Data Analysis Pipeline. *PLoS Comput Biol.* 2016;12(9):e1005112.
67. Levine JH, Simonds EF, Bendall SC, Davis KL, Amir el AD, Tadmor MD, et al. Data-Driven Phenotypic Dissection of AML Reveals Progenitor-like Cells that Correlate with Prognosis. *Cell.* 2015;162(1):184-97.
68. Dufort MJS, Cate; Linsley, Peter S. Cell type–specific immune phenotypes predict loss of insulin secretion in new-onset type 1 diabetes. *JCI Insight.* 2019;4(4).

# Figures

Figure 1

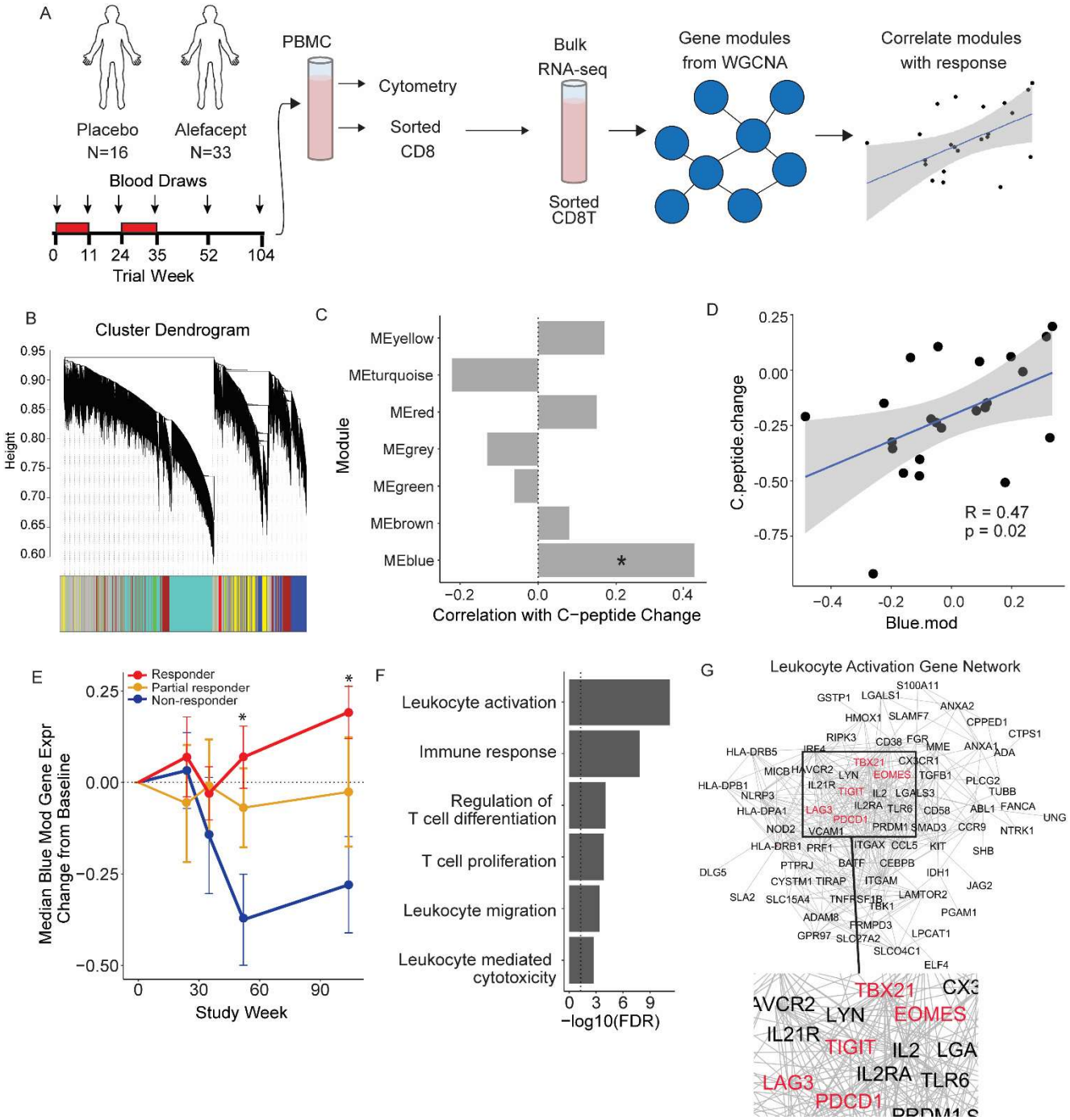


**Figure 1. CD8 T cell activation and exhaustion-associated gene signature was associated with response to alefacept. A)** Schematic diagram shows analysis workflow. **B)** WGCNA cluster dendrogram

is shown for analysis of 5K most variable genes in CD8 samples (n=24; including 2 placebo). **C)** Pearson correlation between module eigengene and C-peptide change. Significance of correlation was determined by Student's asymptotic one-tailed t-test. Only the blue module was significantly correlated with C-peptide change ($p < 0.05$). Correlation and significance calculations included all 24 subjects used for WGCNA module generation. **D)** Graph shows blue module eigengene expression vs C-peptide change at week 104 across the same 24 subjects ($R = 0.47$, $p = 0.023$, FDR = 0.14). Pearson correlation and the corresponding t-test of correlation significance were performed using cor.test function in R. **E)** Change from baseline median expression of blue module genes in responders, partial responders, and non-responders over time. See Table S1 for sample numbers per group and visit. Significant differences at week 52 and 104 were seen between responders and non-responders. Significance was determined by repeated measures ANOVA, with multiplicity adjustment applied to p-values. **F)** A selection of significantly enriched terms identified by gene ontology enrichment analysis of blue module genes are shown with their respective enrichment p-value (-log10(FDR)). **G)** Blue module genes categorized as "leukocyte activation" by GO analysis were clustered using string (string-db.org) and visualized in Cytoscape. Inhibitory marker names colored red.

Figure 2

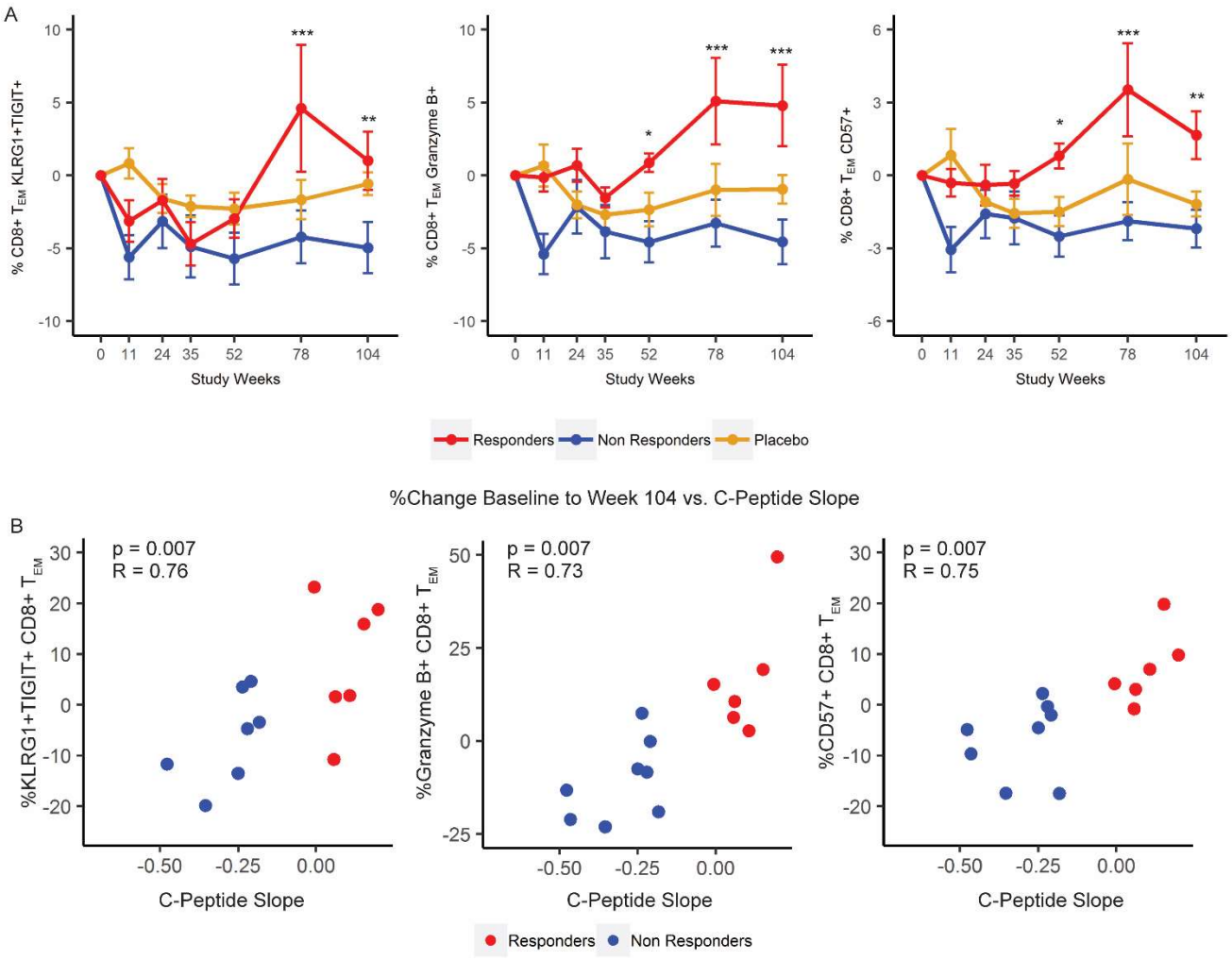


**Figure 2. Increased frequency of memory CD8 subsets correlated with beneficial response to alefacept. A)** Longitudinal analysis of KLRG1+TIGIT+, Granzyme B+, and CD57+ is shown as the change from baseline percentage of CD8+ TEM in responders (n=7; red), non-responders (n=9; blue), and placebo (n=12; yellow). Differences between groups were analyzed by Repeated Measure (RM) ANOVA with baseline adjustment and Bonferroni multiple comparison correction. P values <0.05 were considered significant. C1; Cycle 1, C2; Cycle 2 of treatment. **B)** Plot shows correlation of the C-peptide change with the change of %KLRG1+TIGIT+, Granzyme B+, and CD57+ CD8+ TEM from baseline to week 104 in responders (n=6) and non-responders (n=7). Spearman correlation were performed with FDR adjustment for multiple comparison.

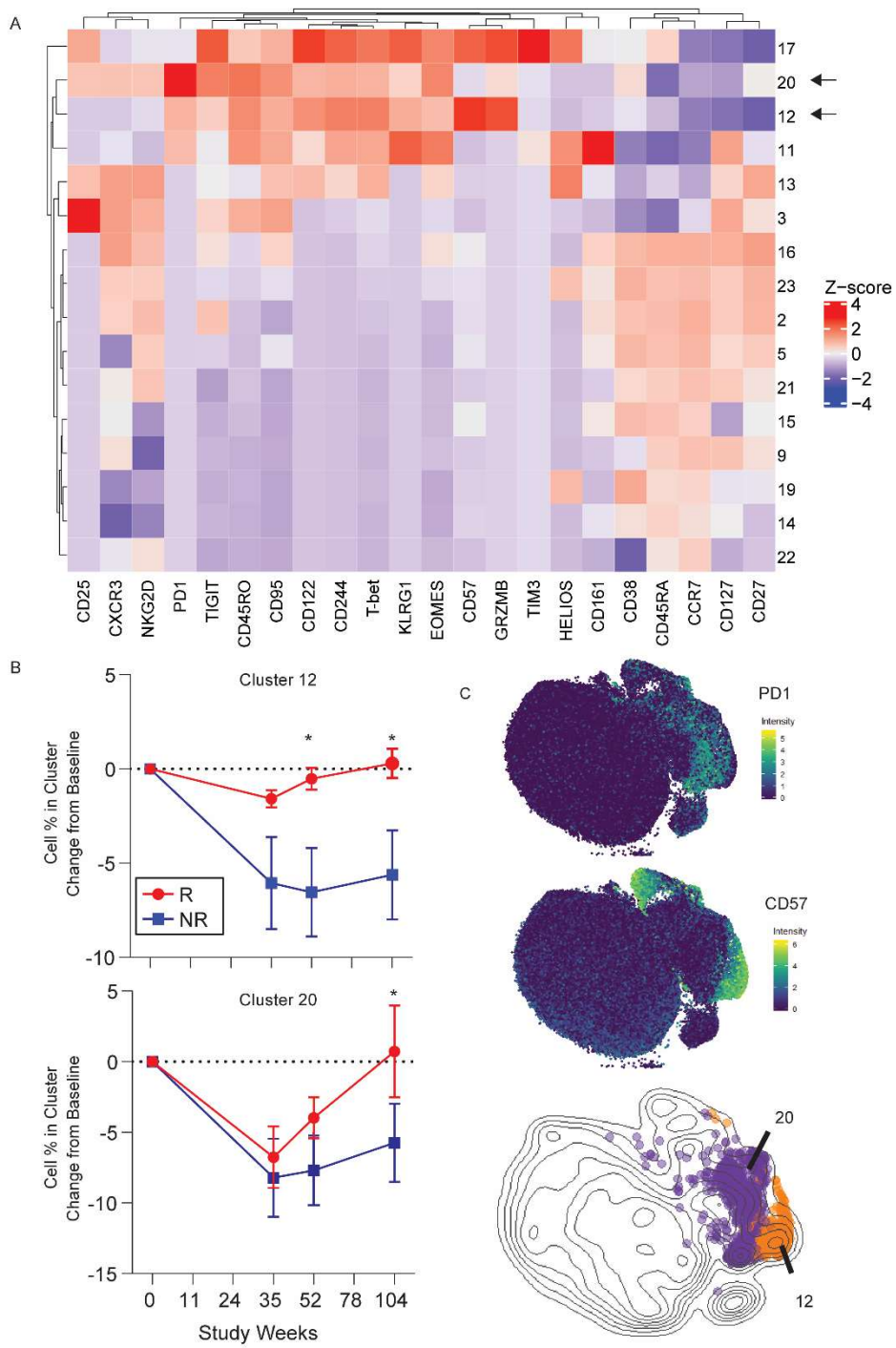


**Figure 3. Two CD8 memory T cell subsets identified by CyTOF analysis were associated with beneficial response to alefacept. A)** Heatmap shows median expression for each cluster that contained at least 1% of total cells. Color indicates column z-score calculated from cluster median expression. Arrows denote the two IR-high clusters that correlated with response, clusters 12 and 20. Analysis included 12 subjects (6 R; 6 NR). **B)** Change from baseline percent of cells in clusters 12 and 20 plotted over time in 6 responders (R) and 6 non-responders (NR). Differences between groups were analyzed by Repeated Measure (RM) ANOVA with baseline adjustment and FDR multiple comparison correction. P

values <0.05 were considered significant. **C)** tSNE was used to visualize CyTOF data at single-cell level. Expression intensity (asinh of MI) is colored on tSNE plots for PD1 and CD57 (top). Overlay of cluster 12 and 20 cells shown on density plot, color-coded as orange and purple, respectively (bottom).

Figure 4

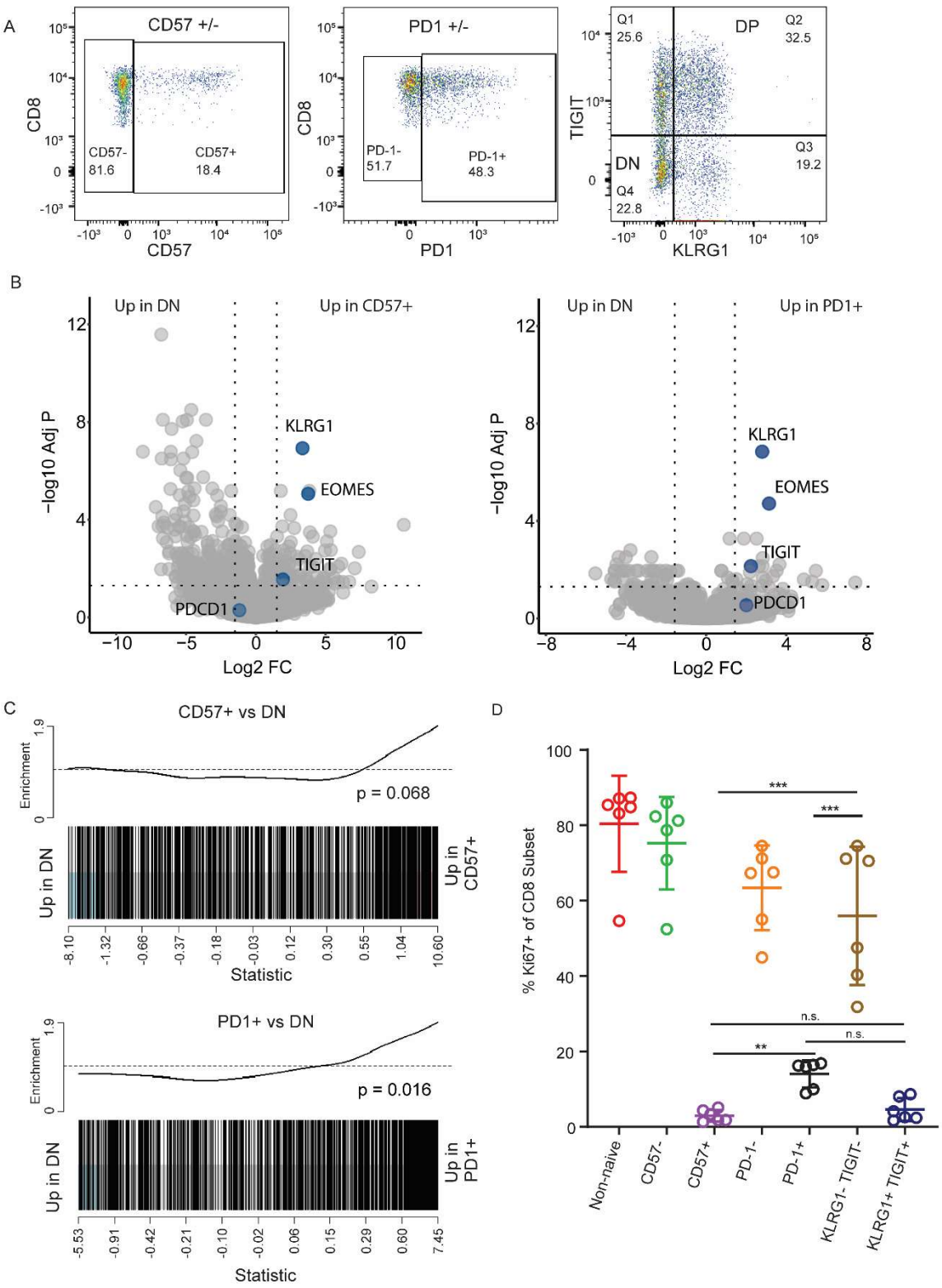


**Figure 4. CD57+ and PD-1+ response-associated CD8 T cells were hypo-proliferative and expressed features of exhaustion. A)** Representative dot plots illustrate sorting strategy to isolate memory (non-naïve CD8 excluding CD45RA+ CCR7+) CD8+ T cell populations (CD57+/-, PD-1 +/-, and

KLRG1/TIGIT +/-). **B)** Volcano plots show differentially expressed genes contrasting PD-1+ (right) and CD57+ (left) with DN cells. Genes canonically associated with exhaustion, as well as key markers of clusters 12 and 20, are highlighted and labeled. **C)** Enrichment barcode plots contrast CD57+ and PD-1+ populations with KLRG1/TIGIT negative (DN) cells in their expression of blue module genes. P-value from rotation gene set analysis *roast* in R. **D)** Ki67+ cell frequency in each of the sorted CD8 subsets (week 104 samples; n=6) following 4 days of stimulation with plate-bound anti-CD3/soluble anti-CD28. Bars indicates median and standard error. P-values were calculated using one-way ANOVA, and results are displayed for comparisons of CD57+, PD-1+ and KLRG1- TIGIT- (DN) frequencies.

Figure 5

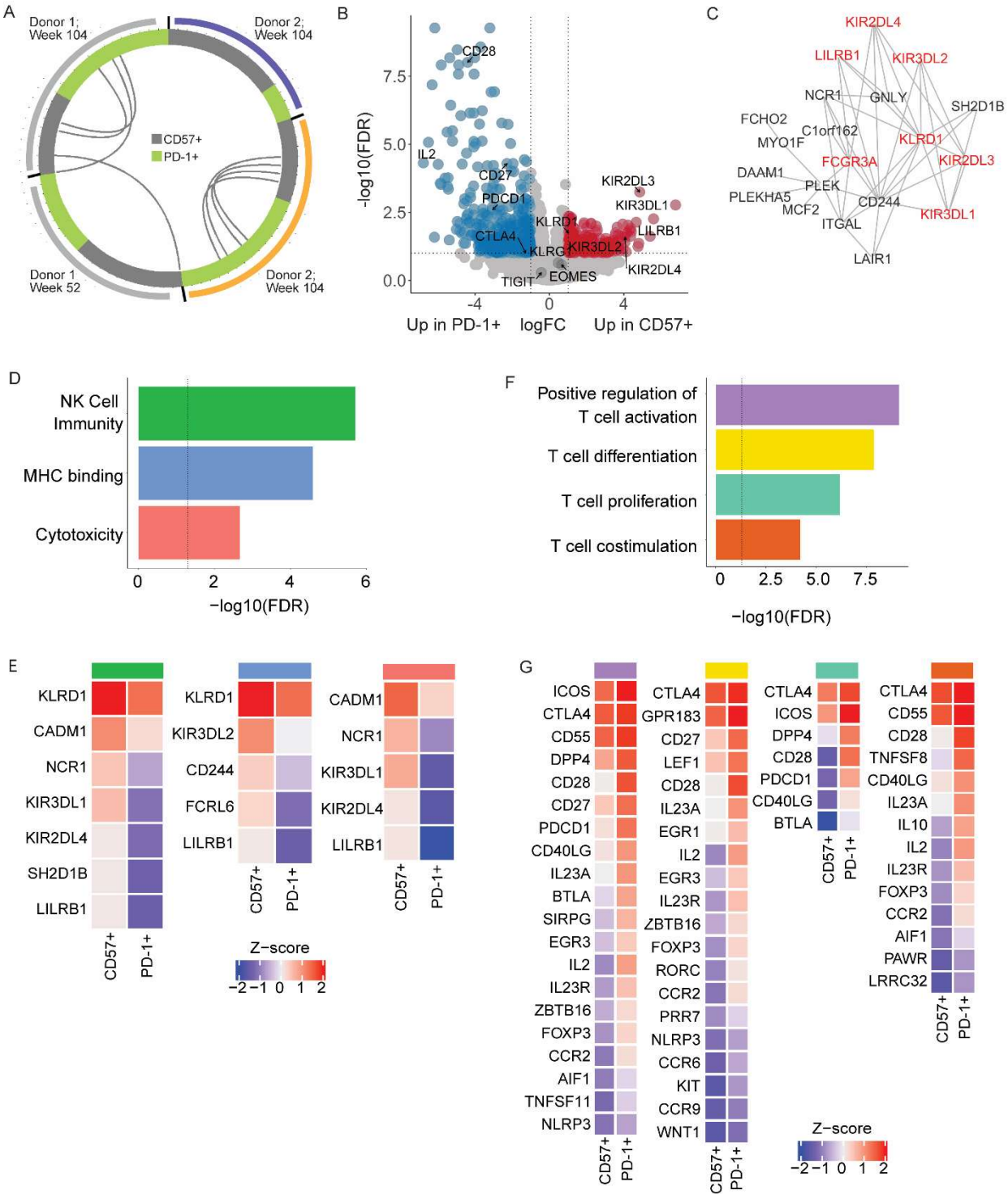


**Figure 5. CD57+ and PD-1+ T cells shared a subset of TCRs but differentially expressed features of NK cytotoxicity and T cell activation. A)** Each segment of Circos plot represents a TCR junction found in PD-1+ (green) or CD57+ (gray) cells from the 4 sorted samples. Color bars denote donors. Arcs connect junctions shared between samples. **B)** Differentially expressed genes identified by limma analysis contrasting PD-1+ (left) and CD57+ (right) cells. Genes whose differential expression reached

significance are highlighted in blue and red (logFC > 1; BH adjusted p < 0.1). **C)** Network shows connected network of genes expressed significantly higher in CD57+ than PD-1+ cells. Key NKRs are highlighted in red. **D)** Selection of enriched pathways in CD57+ cells are shown with respective significance of GO term gene over-representation in set. **E)** Relative expression of pathway-associated genes in CD57+ and PD-1+ cells, calculated as the mean scaled expression of the gene across all samples. **F)** Selection of enriched pathways in the genes differentially expression in PD-1+ cells, determined as in (D). **G)** Relative expression of pathway-associated genes in PD-1+ and CD57+ cells, analyzed as in (E).

| | Bulk CD8 RNA-seq<br>n (% of cohort) | CyTOF<br>n (% of cohort) | Flow Cytometry<br>n (% of cohort) |
|---|---|---|---|
| **Age group** | | | |
| 12-15 years | 5 (19%) | 3 (25%) | 3 (19%) |
| 16-35 years | 21 (81%) | 9 (75%) | 13 (81%) |
| **Sex** | | | |
| Female | 12 (46%) | 5 (42%) | 7 (44%) |
| Male | 14 (54%) | 7 (58%) | 9 (56%) |
| **Response Group** | | | |
| Responder | 7 (27%) | 6 (50%) | 7 (44%) |
| Non-responder | 9 (35%) | 6 (50%) | 9 (56%) |
| Partial responder | 10 (38%) | 0 | 0 |
| **Total n in cohort** | 26 | 12 | 16 |

**Table 1. Cohort demographics for RNA-seq and cytometry analyses.** Values indicate n of cohort (% of total n of cohort). RNA-seq sample numbers indicate the number of subjects with data at one or more visit after filtering low quality libraries. Cohort subsets did not differ significantly in age, sex, or response than the complete alefacept treated cohort (n=33) described in Rigby et al, as determined by Fisher's exact test.